

# **Developing a detection and monitoring framework for wildfire regimes with L-Band Polarimetric SAR**

**Karen An<sup>1</sup>, Cathleen E. Jones<sup>1</sup>, and Yunling Lou<sup>1</sup>**

<sup>1</sup>Jet Propulsion Laboratory, California Institute of Technology, Pasadena, CA 91109, USA.

Corresponding author: Karen An (karen.an@jpl.nasa.gov)

## **Key Points:**

- Polarimetric radar products can offer supplementary information on fuel load, past fire scars, and vegetation recovery.
- The alpha angle from eigenvectors better separates burn severity classes, while HV polarization better identifies burned from unburned area.
- Long-term monitoring with a similar L-band instrument can be achieved once the upcoming NISAR sensor is fully operational.

## Abstract

Many communities coexist with wildfires that can lead to loss of lives, property, and ecosystem services. The increasing usage of remote sensing tools to aid disaster response and post-event assessment offers fire agencies an opportunity for additional surveillance. The adaptability of radar instruments in their ability to see through smoke, haze, and clouds during the day or night is especially relevant when cloud cover or lack of solar illumination inhibits traditional visual surveys of damage. The Station (2009) and Bobcat (2020) Fires are the two largest fires in Los Angeles County history, each burning over 100,000 acres. These areas are imaged with NASA's UAVSAR (Uninhabited Aerial Vehicle Synthetic Aperture Radar) L-band synthetic aperture radar. For these neighboring fires, we investigate the usage of polarimetric radar products to detect fire scars, burn severity, and different fuel (vegetation) types. These fire characteristics are observed using individual HV (horizontally emitted, vertically collected) images and in eigenvector decomposition products derived from quad-polarimetric data. Traditionally unintuitive, yet powerful PolSAR (polarimetric SAR) products are moved into GIS-friendly (geographic information system) formats to be analyzed alongside agency data such as fire perimeters, burn progression outlines, and soil burn severity. We demonstrate the advantages of combining PolSAR with GIS datasets and methods to understand the fuel loads which contributed to the fires and to monitor post-fire vegetation recovery.

## Plain Language Summary

Wildfires around the world lead to loss of lives, property, and environmental benefits. The increasing usage of satellite imagery to aid disaster response and monitoring offers fire agencies an opportunity for additional surveillance. Radar instruments are able to see through smoke, haze, and clouds during the day or night, which is especially relevant when cloud cover or weather conditions block traditional visual surveys of damage. The Station (2009) and Bobcat (2020) Fires are the two largest fires in Los Angeles County history, each burning over 100,000 acres. These areas were imaged with NASA's UAVSAR (Uninhabited Aerial Vehicle Synthetic Aperture Radar) radar, an airborne sensor with high quality measurements and detailed resolution. For these neighboring fires, we investigate the usage of radar remote sensing to detect fire scars, burn severity, and different fuel (vegetation) types. These fire characteristics are observed using a variety of polarimetric radar products. These products are analyzed alongside agency data such as burned area outlines, burn progression outlines, and burn severity. We demonstrate the advantages of using radar datasets to understand the vegetation which contributed to the fires and to monitor post-fire recovery.

## 1 Introduction

Although fires play a natural role for key ecosystem services, local fire regimes have been greatly impacted by human activity. Many communities coexist with fire-prone areas that can lead to loss of lives, property, and ecosystem services (Moritz et al., 2014). Most deaths and loss of homes occur in the wildland-urban interface, where most fire suppression activities occur as well. Policy response to these negative outcomes usually involves increased fuel reduction and fire suppression. As a result, decades of fire suppression in the western U.S. have possibly altered prehistoric fire regimes (Perry et al., 2011). Knowledge of the local fire regime not only helps to protect populations residing in this interface, but also offers insight for management of

these areas (e.g. prescribed burning, fuel treatments, etc.). In the face of increasing wildfire intensity and frequency due to climate change, a more sustainable coexistence with wildfire should be achieved (Mortiz et al., 2014).

The local fire regime is unique to each region's climate, topography, vegetation, and other environmental characteristics. Understanding how these factors contribute to fuel load, burn severity, and burn progression helps infer the likely formation of future fires within the regime. Wildland fuel is defined as the vegetative material or biomass that burns in a wildfire (Pynes, 1984). Fuel load is not the direct cause of wildfires, but can affect fire area and severity. Fuel load changes can be caused by human and natural disturbances, weather, and seasonal plant cycles. In the western U.S., fire severity is found to increase with fuel load, based on actual evapotranspiration (AET) rates as a representation for fuel amount (Parks et al., 2014). Maps of fuel load over large areas can help fire managers identify hotspots across jurisdictions. The amount of available fuel is also dependent on the fuel moisture, the amount of water present in the fuel (Pynes, 1984). This measurement is of interest since low dead fuel moisture allows for a higher rate of fire spread.

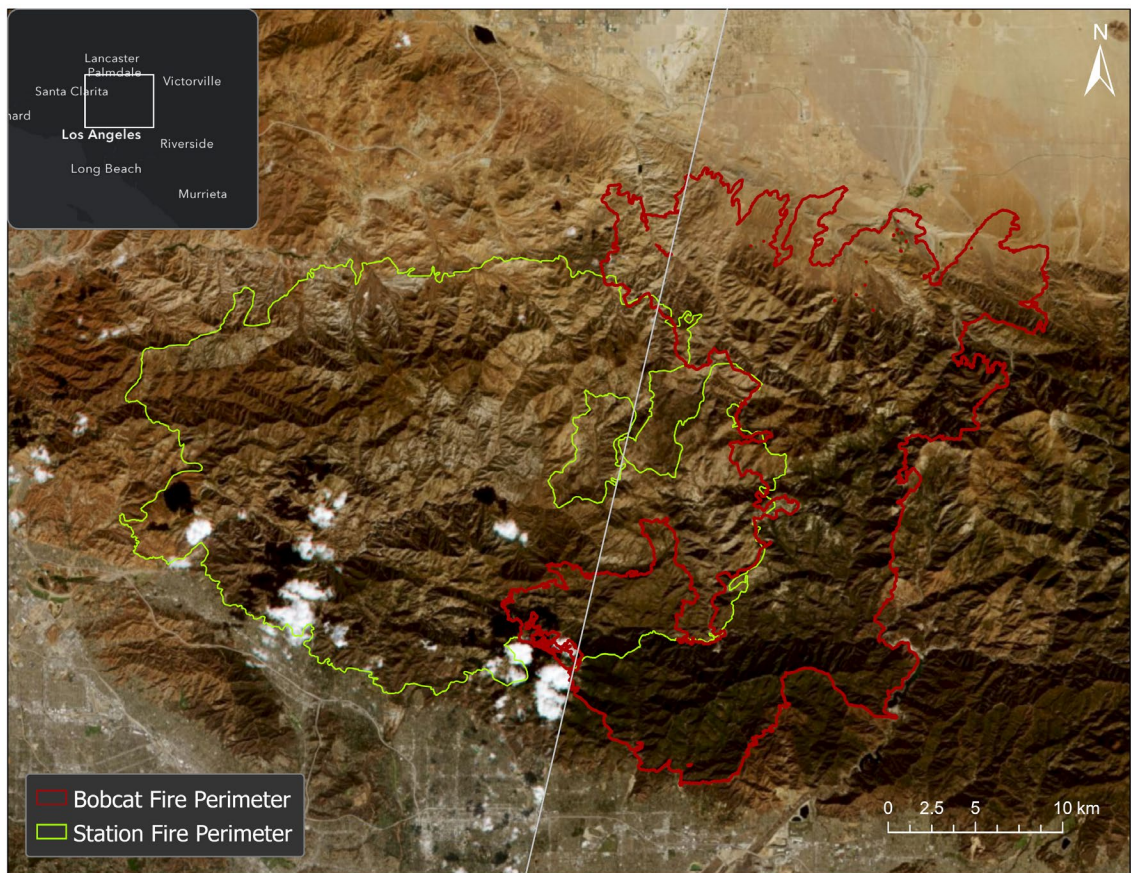


**Figure 1.** Study area of the Angeles National Forest in Los Angeles County, California with the Bobcat Fire perimeter (red) and Station Fire (green). The gray diagonal line separates Planet imagery (RapidEye Scene Product) acquired on October 7, 2018 to the left, and imagery acquired on October 19, 2018 to the right.

77       The severity, frequency, and area affected by wildfires globally has increased over the  
78 past few decades (Hallema et al., 2018). In the western U.S., drier conditions from climate  
79 change, extreme temperatures, and variable precipitation can increase wildfire severity (Crockett  
80 et al., 2018). Increased temperatures during spring and summer allow early snowmelt, leading to  
81 higher frequency of wildfires (Westerling et al., 2006). In southern California, the two largest  
82 wildfires in Los Angeles County history, Station (2009) and Bobcat (2020) Fires, occurred in  
83 Angeles National Forest, each burning >110,000 acres and threatening the populations,  
84 structures, and air quality of nearby communities. The Station Fire began on August 26, 2009,  
85 and burned over 160,000 acres in 50 days, threatening 12,000 homes/structures and resulting in  
86 the deaths of two firefighters (Los Angeles Times, 2019). According to an L.A. County Fire  
87 spokesperson, the large fuel volume was a major reason for the size and spread of the Station  
88 Fire. Then, nearby Bobcat Fire started burning on September 6, 2020, likely a result of a power  
89 line ignition. The fire burned over 115,000 acres until 92% contained by October 17, 2020 (U.S.  
90 Forest Service). In this region, drought is an important determinant of available fuels. The lower-  
91 than-usual fuel moisture during drought conditions results in higher fuel availability, higher fire  
92 intensity, and more difficult fire suppression (Pynes, 1984). For live fuels such as the drought-  
93 resistant brush and chaparral that populates the area, fuel moisture can lower to 40-50% during a  
94 drought (Pynes, 1984). This can lead to total plant mortality during a prolonged and severe  
95 drought, which contributes to dead fuel amount. Knowing the fuel load of chaparral is especially  
96 important because live chaparral leaves contain a certain chemistry and structure that increases  
97 its combustibility (Dennison et al., 2000).

98       The increasing usage of remote sensing tools to aid disaster response offers fire agencies  
99 an opportunity for additional surveillance. Optical imagery (French et al., 2008; Van  
100 Wagtendonk et al., 2004), as well as multi- and hyper-spectral imagery (Hislop et al., 2018;  
101 Lewis et al., 2011; Veraverbeke et al., 2010), have been shown to detect fire occurrence, burn  
102 severity, and burned area. However, smoke and weather conditions can impede current  
103 monitoring methods which rely on field survey and optical imagery. For chaparral-populated  
104 areas such as Angeles National Forest, fully characterizing fuel load from optical imagery can  
105 also be limited because the short wavelengths of the visible and near-infrared spectrum are more  
106 easily scattered or absorbed by the canopy (Dennison et al., 2000).

107       Fire management and response can be aided by radar remote sensing products in addition  
108 to traditional survey methods. Radar remote sensing has the potential to better characterize local  
109 fire regime, including its fuel load over time. This is due to the physical relationship between  
110 radar backscatter and forest structure and biomass, as scattering can be dependent on all  
111 components of biomass: branches, stems, leaves, and also moisture content. In recent years,  
112 research applying polarimetric products to characterize the fire regime is emerging (Czuchlewski  
113 et al., 2005; Nunziata et al., 2021; Ban et al., 2020; Rao et al., 2020), but studies usually only  
114 reference products from space sensors with lower spatial resolution and do not quantify metrics  
115 such as burn severity or fuel load. Parker et al. (2021) does explore an archive of high spatial  
116 resolution L-band products, but only visually analyzes the fire scars in the Angeles National  
117 Forest over the past decade. To help aid response agencies for future fires in the area, we  
118 quantitatively evaluate the usage of L-band polarimetric radar products to detect fire scars, burn  
119 severity, and vegetation recovery, including separation by different fuel (vegetation) types. In  
120 this way we examine the information available for pre-, active, and post-fire management.

## 2 Data and Methods

### 2.1 L-Band Polarimetric Data

The Uninhabited Aerial Vehicle Synthetic Aperture Radar (UAVSAR) sensor from NASA is an airborne radar which collects high resolution, quad-polarimetric products for various scientific applications. The UAVSAR instrument flies as a pod attached to a Gulfstream-III aircraft, and is an L-band (23.8 cm wavelength) airborne sensor with high signal-to-noise ratio and repeat flight track accuracy (Hensley et al., 2011). The instrument operates at an altitude of 12.5 km, with a bandwidth of 80 MHz and a center frequency of 1.2575 GHz. The image swath is 22 km wide, and the left-side-looking incidence angles range from 22°–67°. The instrument spatial resolution is 0.8 m (along flight-line) by 1.7 m (along the line-of-sight (LOS)) without multi-looking (Bekaert et al., 2019). The benefits of radar instruments include their ability to see through smoke, haze, clouds, and that data can be collected during the day or night. This adaptability is especially relevant for hazy skies during a wildfire, which inhibit traditional visual surveys of damage. The UAVSAR system can be deployed after a disaster event to deliver pertinent information to decision makers. Many parts of California have previously been imaged, providing some pre-fire data sets.

UAVSAR offers fully polarized products as ground projected files, which contain georeferenced multi-looked data for all six cross-products of the scattering matrix (HHHH, HVHV, VVVV, HHHV, HVHV, and HVVV) in linear power units. Polarized backscatter waves contain information on geometry, reflectivity, shape, roughness, and orientation of objects. For this study, the HVHV polarization is predominantly used to highlight the presence of healthy vegetation. HV denotes a horizontally emitted, vertically received polarization and we use ‘HV’ as shorthand for the HVHV product in the rest of this document. A difference of two HV images can be used to determine the changes in vegetation between acquisitions. SAR side-looking geometry can lead to geometric and radiometric distortions due to varying surface slopes. Since the Angeles National Forest contains mountainous terrain, a radiometric terrain correction (RTC) is applied to the HV datasets. Since terrain in radar shadow makes the illuminated area very small, the correction factor cannot be applied in these areas. There exist other cases as well for which the local geometry makes correction difficult and the correction factor lies outside specified limits. The RTC algorithm is provided by Simard et al. (2016) and applied to improve backscatter estimates, removing geometric distortions and any terrain in radar shadow. These shadowed areas are evident in this paper’s figures as missing terrain features in grey.

This study area is partially covered by UAVSAR flight line SanAnd\_08525 for the following dates: 10/11/2018, 09/18/2020, 10/15/2020, 05/26/2021, and 11/17/2021. These dates allow a comparison of pre-fire, active, and post-fire conditions for Bobcat Fire. Corresponding 2020 dates for the flight line to the immediate north, SanAnd\_08527 (02/05/2018, 09/18/2020, and 10/14/2020) are also used to complete the study area. Data for the northern flight line was not collected during 2021.

### 2.2 Polarimetric Decomposition

Cloude-Pottier (H-A-Alpha) decompositions (Cloude & Pottier, 1997; Pottier & Ferro-Famil, 2012) are typically performed on the fully polarized products to extract further scattering information beyond that of the HV polarization product. The PolSARpro program from the European Space Agency (ESA) can ingest UAVSAR data to generate eigen-products from the H-A-Alpha decomposition, namely Eigenvector 1 (also called Alpha Angle 1), Eigenvalue 1,

166 entropy, anisotropy, and mean alpha angle products used to classify the scattering mechanisms.  
 167 These products are discussed below, and a corrected bug in the PolSARpro routine to generate  
 168 the T3 coherency matrix is discussed in the Supporting Information (Text S1).

169       Alpha Angle 1 (from Eigenvector 1) describes the type of dominant scattering (surface,  
 170 volume, double-bounce) present. Surface scattering ( $0^\circ$ ) tends to occur on smooth surfaces like  
 171 water, and increases with roughness; volume scattering ( $45^\circ$ ) is found in vegetated areas like  
 172 forests; and double-bounce ( $90^\circ$ ) is most common in urban areas containing vertical structures.  
 173 Eigenvalue 1 measures the intensity of scattering described by Eigenvector 1. Eigenvectors and  
 174 Eigenvalues 2 and 3 are also automatically extracted, representing secondary and tertiary  
 175 scattering mechanisms, but are not included directly in this study. Derived from all three  
 176 eigenvalues, entropy (H) represents the degree of randomness caused by different scattering  
 177 mechanisms and takes values from 0 to 1. Anisotropy (A), also derived from the eigenvalues,  
 178 describes the importance of the secondary scattering mechanisms and also ranges from 0 to 1.  
 179 Lastly, the mean alpha angle (Alpha), derived from the eigenvectors, describes the average  
 180 scattering mechanism (single, volume, and double-bounce). The mean alpha angle is the  
 181 weighted average from Eigenvectors 1-3. Taken together, these polarimetric decomposition  
 182 products help quantify the scattering intensities and types for areas with changing vegetation and  
 183 moisture, such as those experiencing wildfires. See the supporting information for images of  
 184 these products for the Bobcat Fire (Figure S1-S6).

## 185 2.3 NISAR-Simulated Data

186       The upcoming NASA-ISRO Synthetic Aperture Radar (NISAR) space mission uses the  
 187 airborne UAVSAR instrument as its prototype for the L-band sensor. NISAR will offer high  
 188 resolution interferometric and polarimetric SAR products on a global scale at regular intervals.  
 189 To preview the mission's products, the UAVSAR team has generated NISAR-simulated datasets  
 190 from original UAVSAR acquisitions (<https://uavsar.jpl.nasa.gov/>). The simulated products are  
 191 derived from the UAVSAR SLC (single look complex) files by reducing spatial resolution and  
 192 adding noise to mimic NISAR's larger antenna (coarser resolution) and longer range (lower  
 193 signal-to-noise ratio). For this study, the HVHV product from the 129A (20 MHz bandwidth) is  
 194 used to compare directly with the HVHV product from UAVSAR (80 MHz bandwidth). The  
 195 129A mode orthorectified product has 9.72 meters ground range spacing. These products are  
 196 multiplied by an accompanying RTC file, which uses the same algorithm described above for  
 197 direct comparison. All PolSAR products described thus far are compatible with Esri's ArcMap  
 198 software for further spatial analysis alongside ancillary GIS data.

## 199 2.4 Geographic Information System (GIS) Datasets

200       A collection of GIS datasets accompanies the evaluation of the UAVSAR and NISAR  
 201 products. Fire perimeters, for Bobcat Fire and all historic fires in the area, are available from the  
 202 U.S. Forest Service (Wildland Fire Interagency Geospatial Services (WFIGS) Group). These  
 203 detailed polygons allow for accurate comparison of burned versus unburned areas seen in the  
 204 PolSAR imagery. A detailed vegetation species map is also used to characterize the area. The  
 205 GAP/LANDFIRE National Terrestrial Ecosystems dataset is a 30 x 30 m raster product from  
 206 2011 containing land use classes represented at very fine thematic detail (U.S. Geological Survey  
 207 (USGS), 2016). The elevation values of the area are provided by the UAVSAR height file  
 208 ancillary product, which is used to calculate the slope value with Esri ArcMap's Slope tool (see  
 209 Supporting Information, Figure S7).

A soil burn severity map is also used to compare loss of vegetation. The burn severity map is provided and field-validated by a U.S. Forest Service Burned Area Emergency Response (BAER) team, and derived from optical Sentinel-2 imagery (U.S. Forest Service, 2020). The near-infrared and mid-infrared spectral bands highlight areas of healthy green vegetation and bare/rocky areas with little vegetation, respectively. In making the severity map, pre- and post-fire scenes are subtracted to develop a differenced Normalized Burn Ratio (dNBR) map. The values are thresholded into unburned/very low, low, moderate, and high burn severity classes, adjusted based on ground conditions. dNBR portrays the variation of burn severity and captures the combined effects of wildfire to both vegetation and underlying soil. A study of fire activity in the western U.S. found high dNBR values indicate an increase in char and scorched vegetation, and a decrease in moisture (Parks et al., 2014).

## 2.5 Sources of Error and Uncertainty

There are a few expected error sources associated with polarimetric backscatter to be discussed, but their full quantification is beyond the scope of this study. Temporal variability can alter backscatter measurements, based on pixel size, temporal resolution, and biomass characteristics. Polarimetric backscatter measurements can be affected by environmental changes such as: weather conditions, soil moisture, vegetation type, and other above ground conditions. Instrument-based errors such as speckle, thermal, and multiplicative noise can be calculated using the number of looks and the ratio of the signal to total noise, SNR (Hensley et al., 2013). Calibration errors can also arise during the conversion of raw signals into calibrated data values (Fore et al., 2009; Hensley et al., 2013). The calibration accuracy of UAVSAR polarimetric intensity products is 0.5 dB relative between different polarizations, and 1.0 dB absolute. The results are visualized with 1 dB bins, commensurate with the calibration accuracy.

Lastly, projected area-induced errors are caused by topographic variations causing changes to pixel area, leading to data artifacts (Hensley et al., 2013). Such effects can be removed using a digital elevation model (DEM), whose quality will affect the area projection being applied to the radar backscatter (Hensley et al., 2013). As discussed above, an RTC algorithm is applied to the UAVSAR datasets to remove topographic areas causing geometric distortions or terrain shadow. Further validation of the vegetation changes observed in the polarimetric data can be achieved with UAVSAR overflights alongside fuel treatments, before, during, and after the burn events.

## 3 Results

The polarimetric radar products derived from the UAVSAR data are presented as most suitable for the three stages of the fire cycle: pre-fire, active fire, and post-fire. As expected, pre-fire and post-fire products have some overlap in utility. This study focuses on the Bobcat Fire, with some analysis of the adjacent Station Fire, and all images are GIS-compatible, overlaid with relevant layers such as fire perimeters.



### 252 3.1 Pre-Fire Stage

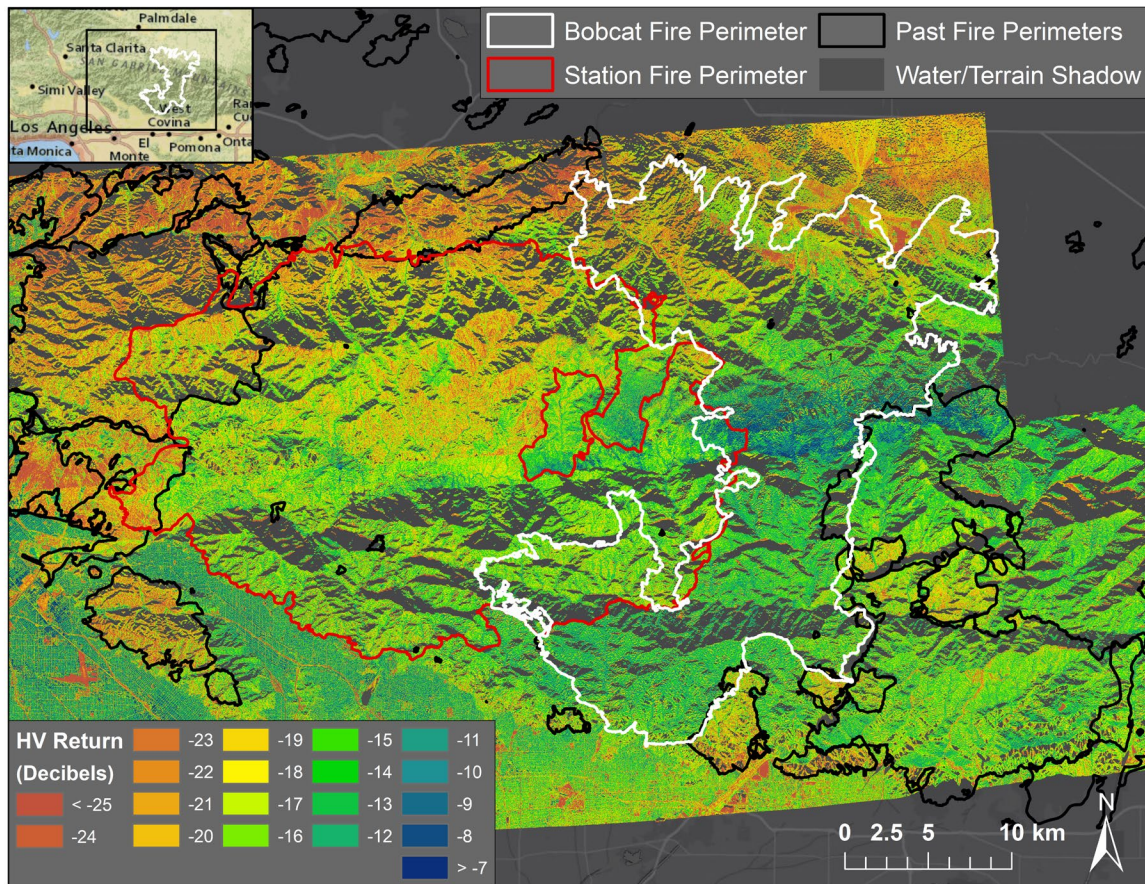


**Figure 2.** HV image from before the Bobcat Fire acquired in February 2018 (northern flight) and October 2018 (southern flight) showing historic fires (black outlines) in the area, including the Station Fire (red outline), which occurred in August 2009. The Bobcat Fire perimeter is shown in white. High HV returns are in green-to-blue colors.

Pre-Bobcat Fire (white perimeter) conditions in October 2018 are observed using single HV images (Figure 2). Orange and red areas indicate low HV return, where less volume scattering, a proxy for vegetation, is present. Green and blue areas highlight high HV values, where a larger amount of healthy biomass exists. Black outlines represent historic fires in the area, overlapping with many low HV areas due to loss of vegetation. The Station Fire (red perimeter) shows a mix of low and high HV return, possibly showing areas of vegetation loss and regrowth, respectively. In order to present results for the entire Bobcat fire perimeter, Figures 2-4 merge two northern and southern UAVSAR flight lines for the study area. Both lines are north-looking, and the overlap region, though visually apparent, only contains an average 3.56 dB difference across the flight line and 0.61 dB difference within the Bobcat perimeter. These small differences are likely due to latitudinal elevation changes, with the northern terrain having higher elevations. The two images were also acquired during different seasons (February 2018 in the north and October 2018 in the south), which results in varying seasonal vegetation changes measured since vegetation tends to be drier (lower HV returns) in October than in February. Nevertheless, the two acquisitions help to provide a complete view of the study area for the entire Bobcat Fire perimeter.



## 274 3.2 Active Fire Stage

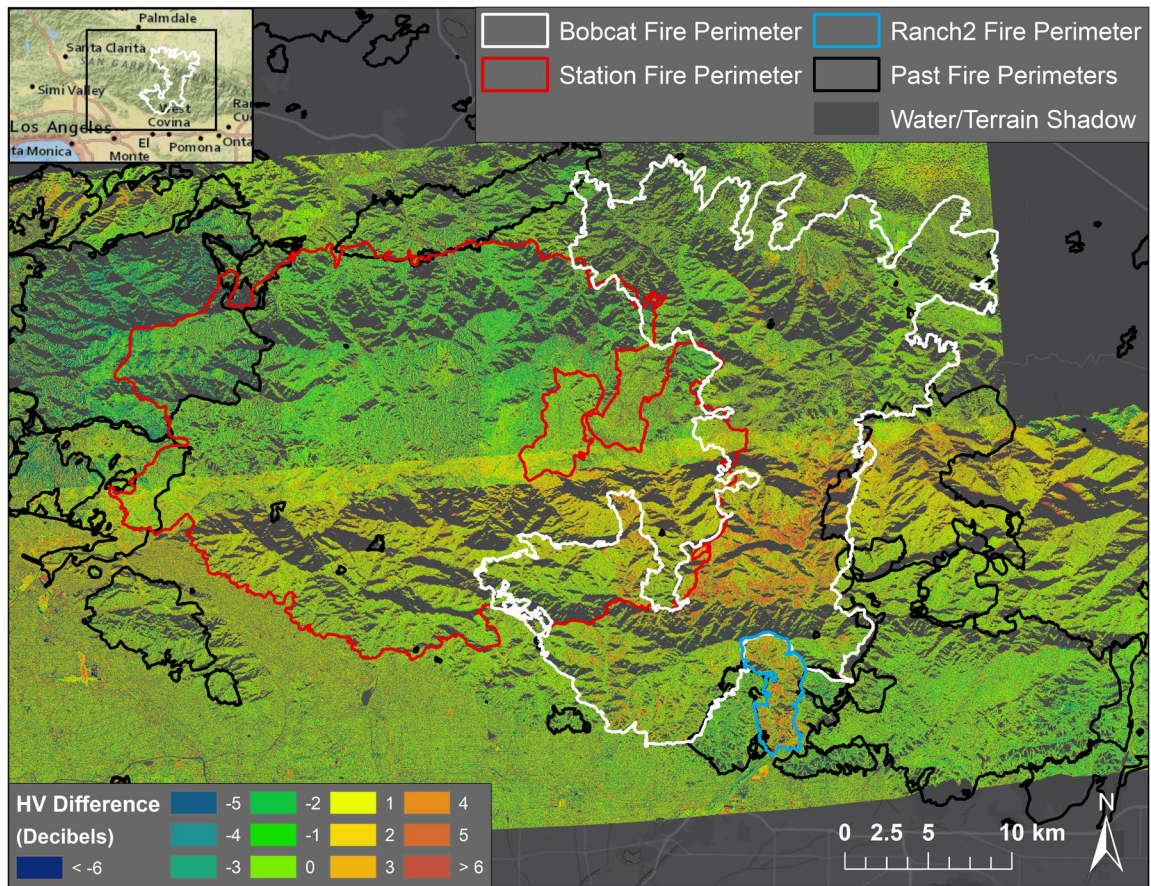


**Figure 3.** HV difference image of February/October 2018 minus September 2020, the later acquired during the active Bobcat Fire. The white outline shows the final Bobcat Fire perimeter from 2020. The Station Fire (2009) perimeter is shown in red and other earlier fires in black. The Ranch2 Fire from August 2020 is also indicated (blue outline, adjacent and to the south of the Bobcat Fire). Large decrease in HV indicates vegetation loss, and appears as red/orange areas in both the Bobcat and Ranch2 perimeters.



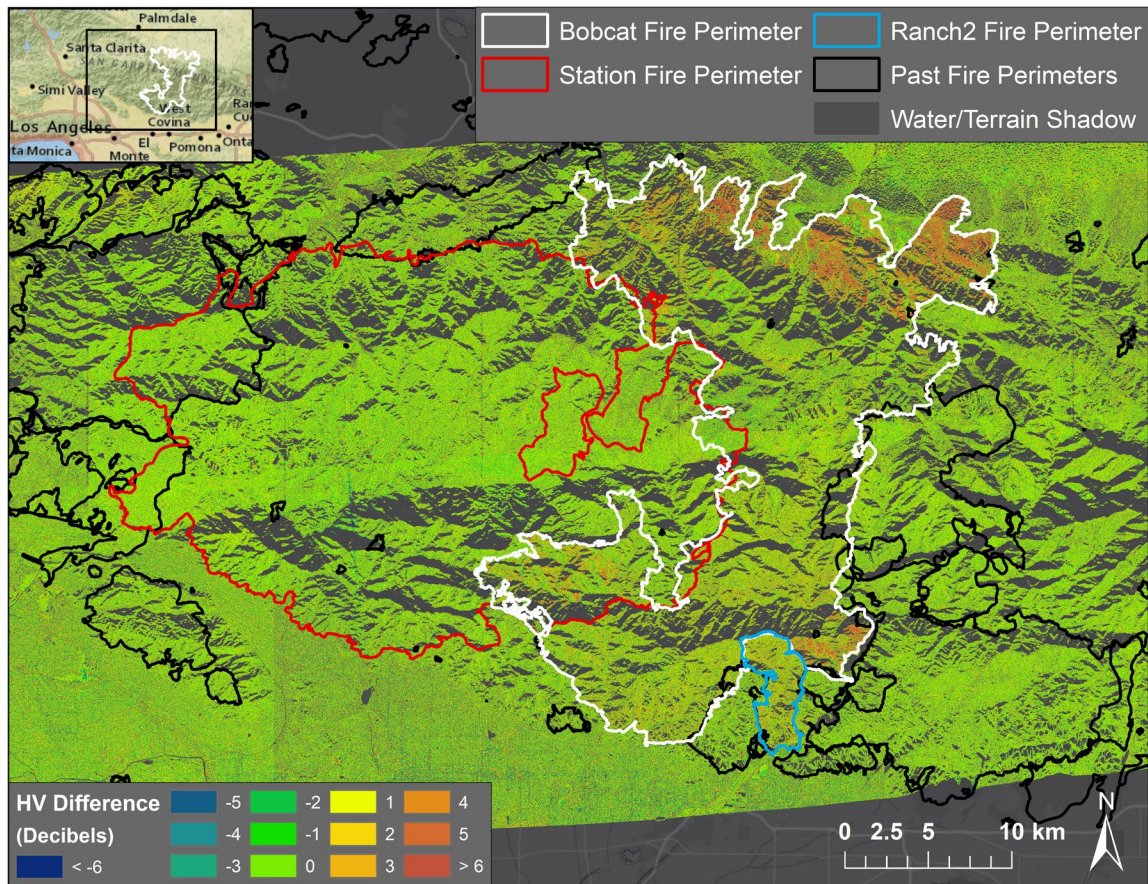


**Figure 4.** HV difference image of September 2020 minus October 2020 showing change during the Bobcat Fire (white outline). The Station Fire (2009) perimeter is shown in red and other earlier fires in black. The Ranch2 fire (blue outline) ended before the September 2020 acquisition. Large decrease in HV (vegetation loss) is shown in red/orange areas.

A simple method to visualize vegetation change over time is to perform a raster difference of two HV images. An HV difference of February/October 2018 (Figure 2) minus September 2020 shows green-colored areas with relatively little change and orange/red areas highlighting a decrease in HV (vegetation) over time (Figure 3). The 2020 image was collected on September 18, twelve days into the Bobcat Fire, which burned until December. High HV differences are found in the center of the final Bobcat Fire perimeter, as also seen in optical imagery (see Figure 9). Some small areas of HV loss are seen in the northern portion of the fire perimeter, but these areas are not yet reported as burned in this time period. These HV differences may be due to natural loss of vegetation from drought conditions during this time. The Ranch2 Fire (blue outline) is also captured, burning over 4,000 acres in August 2020. Within the southern Station Fire perimeter, there is some continued loss of vegetation, possibly due to drought conditions. The border between the north and southern flight lines is more distinct in this first difference image (Figure 3) due to the long temporal difference (two years) between acquisitions. The northern and southern images were collected on the same date in September 2020 and one day apart in October 2020.

The next image was collected on October 15, 2020, while the Bobcat Fire continued, and the September 2020 minus October 2020 HV difference image is shown in Figure 4. In Figure 4,



orange/red areas on the edges of the fire perimeter emphasize the areas that burned during this month, the timing of which is confirmed by the final reported fire progression map (see Figure 10). Most of the difference image is green (showing little change) since the temporal difference is much lower, showing only around a month of vegetation changes. The Ranch2 Fire area also disappears since no major changes occurred within that area during this short time period. Similarly, the regions of past fire (black outlines) show little change in both HV difference images (Figures 3-4), indicating no major vegetation regrowth has occurred during these time periods. There are also vertical streaking artifacts in the HV difference map (Figure 4), which are likely related to known effects from notching the data during processing to reduce radio frequency interference (RFI) (Musgrove et al., 2017).

### 3.3 Post-Fire Stage

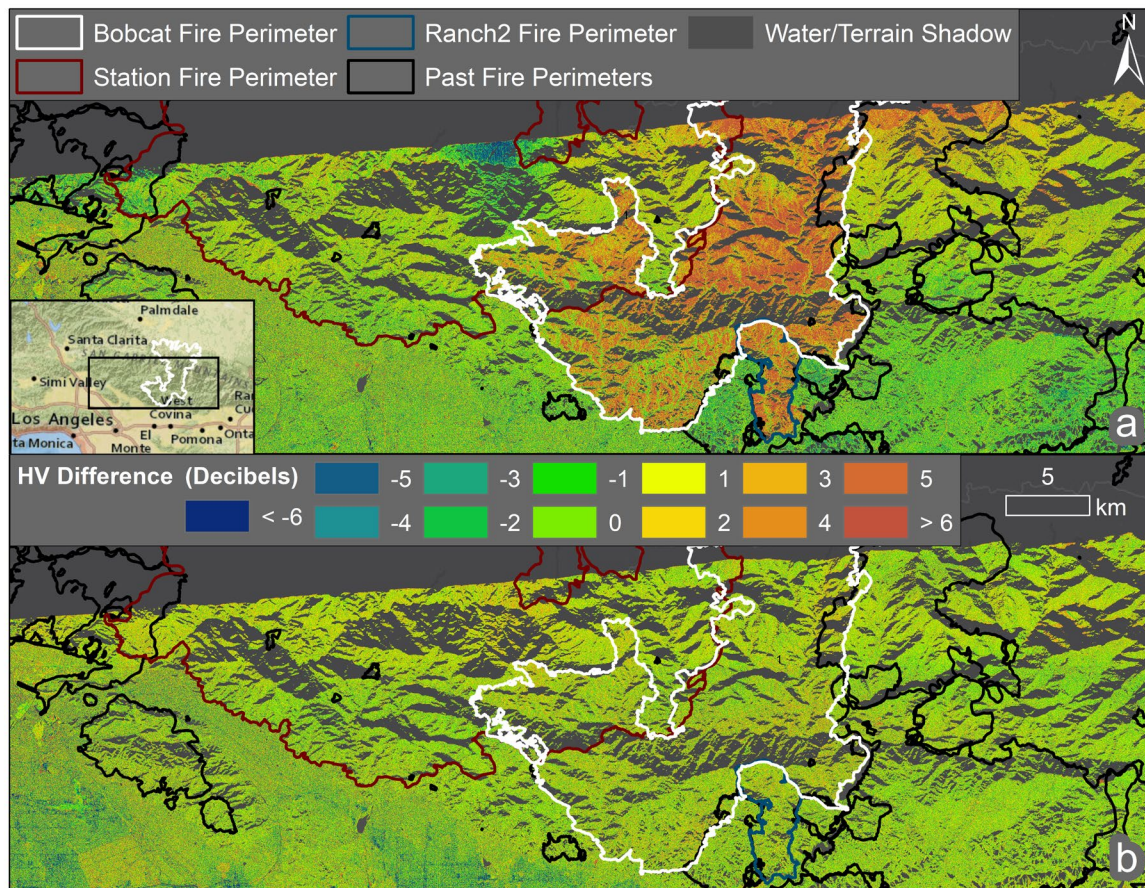


**Figure 5.** (a) HV difference image of October 2018 minus May 2021 for the southern flight line, about six months after the Bobcat Fire (white outline) was contained. High HV loss is shown in red/orange areas. (b) shows the HV difference for May 2021 minus November 2021.

The next UAVSAR flight after the October 2020 acquisition occurred on May 26, 2021. Figure 5a shows the HV difference between October 2018 (Figure 2), before the Bobcat Fire, and May 2021, about six months after the Bobcat Fire. Only the southern line, SanAnd\_08525 is shown because the northern line (SanAnd\_08527) has not been collected since October 2020 at the time of writing. In general, the study area outside the Bobcat Fire is mostly green, showing little vegetation growth since 2020. Some nearby historic fires do appear slightly darker green,

and contain blue areas of HV gain, possibly indicating some regrowth (Figure 5a). The deep orange/red areas of the image represent a loss of HV, and match very well the published final fire perimeter (white outline). There are small areas of inconsistency, where the manually generated fire perimeter includes areas of little HV change as measured by UAVSAR. This disagreement is also observed in the Ranch2 fire perimeter (blue outline). There is also a feature of HV gain (dark green/blue) in the center of the image, located within the Station Fire perimeter (Figure 5a). It is unlikely to be measuring actual vegetation regrowth as this feature shows the remnants of a RFI signal from the 2021 image that has been notch filtered to reduce interference effects. After the May 2021 acquisition, the next and most recent data was collected on November 17, 2021. Around six months after the fire's containment, the difference image in Figure 5b offers a final, SAR-derived burn scar of the Bobcat fire (as well as for Ranch2), which still shows low HV compared to pre-fire conditions, indicating that full recovery has yet to be achieved possibly due to continued drought conditions.

### 3.4 Polarimetric Time Series from Pre- to Post-Fire

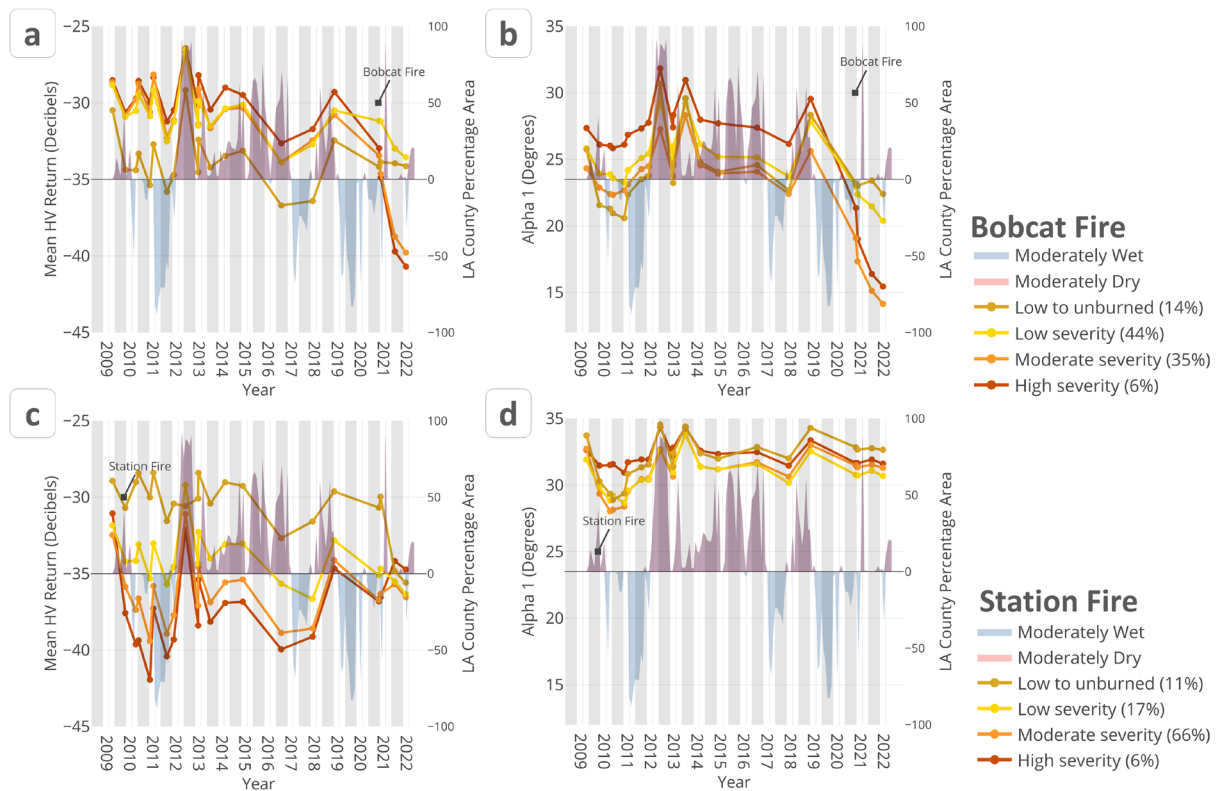


**Figure 6.** Comparison of HV return and Alpha Angle 1 (Eigenvector 1) time series for the Bobcat and Station Fires. All results are derived from the southern UAVSAR flight line (SanAnd\_08525). For the Bobcat Fire, the mean HV return (a) is shown for February 2009–November 2021 for pixels within each burn severity class from optical imagery. Area percentage covered by optical data for each severity class is shown in the legends. The actual pixel count per severity class differs per class and per fire due to terrain shadow. The Alpha Angle 1 is similarly plotted for the Bobcat Fire (b). Panels c and d show the HV and Alpha Angle 1 time series, respectively for the Station Fire.

Further scattering information is extracted from the original UAVSAR polarimetric product. The mean HV value within each burn severity class is shown for the Bobcat (Figure 6a-b) and Station Fires (Figure 6c-d). Each plot only contains values from the pixels within each respective fire perimeter for the southern UAVSAR flight line (SanAnd\_08525). Only this flight line is used to include the 2021 data takes, which were not collected for the northern flight line. Each plot uses the USDA/BAER burn severity classes to mask pixels that fall into each class. The percentage area that each burn severity class covers for each fire is included in the legends, and is only an approximation as each flight date contains a different RTC mask. The HV return is provided by the original UAVSAR dataset, and the Alpha Angle 1 is derived from the H-A-Alpha Eigenvector polarimetric decomposition. The Alpha 1 value measures the dominant type of scattering mechanism: surface (0°), volume (45°), and double-bounce (90°). Both plots contain the history of wet/dry periods as a percentage area (U.S. Drought Monitor) of Los Angeles County and the x-axis intervals coincide with the wet/dry seasons of the study area. The standard error,  $SE = \frac{\sigma}{\sqrt{n}}$ , where  $\sigma$  is the sample standard deviation and  $n$  is the number of samples (or acquisitions), is calculated but too small to be visibly shown. The average standard error for all data points shown for the Bobcat Fire (Figure 6a-b) is 0.016 dB and the average standard error for Station Fire (Figure 6a-b) is 0.00024 dB.

The Bobcat Fire plots (Figure 6a-b) only contain pixels in the southern flight line which overlapped with the Bobcat fire perimeter, covering 41% area of the final burn scar. These plots are not representative of the entire burned area, but do contain the majority of high burn severity areas. The HV return for Bobcat Fire shows that areas which eventually burned at high severity contained one of the highest values from 2009-2020, followed closely by the moderate, low, and unburned severity classes (Figure 6a). The Alpha 1 time series for Bobcat Fire follows a similar pattern, though the separation between lower severity classes is not as distinct and the separation of high burn severity is more distinct (Figure 6b). Before the Bobcat Fire, the high severity area saw the most volume scattering overall compared to the other severity classes. The other severity classes followed a similar pattern, but at smaller alpha angle magnitudes. The small decrease in alpha angle across all classes in 2009 is due to the areas of overlap between the Bobcat and Station Fire, which burned in 2009. The Alpha 1 time series shows better separation from the high burn severity class, while the HV time series shows more distinction between burned and unburned classes. High severity areas also showed the largest decrease post-fire, as expected (Figure 6b). The decrease in other classes is also relative to their severity levels, i.e. the decreasing slope of the moderate severity class is larger than the slope of the low severity class from 2018-2020. A temporal lag from seasonal effects is also evident. For example, there is a gradual increase in volume scattering after the 2011 wet season which does not reach its peak until 2012-2014, during drought year, which subsequently leads to a decrease in volume scattering the following years.

Similar to the previous plots, the Station Fire plots (Figure 6c-d) only contain pixels in the southern flight line which overlapped with the Station fire perimeter, which covers 48% area of the final burn scar. The HV return for Station Fire shows unburned to low burn severity areas with consistently higher HV values over time (Figure 6c). Similar to Bobcat Fire, the high burn severity class for Station Fire contains the largest decline in HV at the start of the fire's occurrence, followed by the less severe classes. High burn severity also begins with the second highest HV value before the Station Fire, indicating more fuel availability. For Alpha 1 (Figure 6d), the entire series is shifted upwards compared to Bobcat Fire (Figure 6b), indicating more



393 volume scattering. Unlike that of Bobcat Fire, there is not much separation among the severity  
394 classes for Station Fire, likely because more moderate burn severity pixels are represented in the  
395 plot relative to the pixel distribution (Figure 6d, see legend). A seasonal lag can also be seen by  
396 the decrease in alpha angle in 2009 during the fire, and gradual regrowth during and after the  
397 2011-12 wet period. Directly after both fires, the alpha angle shifts from more volume scattering  
398 towards more surface scattering. The high severity areas do not show the largest decrease once  
399 the Station Fire started burning in 2009, but this is likely due to terrain shadow in these areas of  
400 the southern flight line leading to low data availability (Figure 6d). The moderate severity class,  
401 covering the most area, shows the largest decrease in volume scattering. During the drought  
402 years of 2012-2016, both fires show slightly decreasing alpha angle, with some recovery after the  
403 2017 wet period. There is then a large data gap between 2018-2020 during which the area was  
404 not imaged by UAVSAR. Due to the overlap in area, the Station Fire plot (Figure 6d) also shows  
405 a decrease in volume scattering after the Bobcat Fire, but the decrease is not as dramatic as  
406 within the Bobcat Fire (Figure 6b).

407 From the two 2021 data takes, there is not much indication of vegetation regrowth for the  
408 Bobcat Fire, as HV and alpha angle values continue to decrease (Figure 6a-b). All burn severity  
409 classes show a continued decrease in alpha angle in 2021, but the low and low to unburned  
410 severity series have a distinctly higher alpha angle than the moderate and high burn severity  
411 series, at around a 15 degree difference. More data acquisitions are needed to confirm the status  
412 of this area, but a lack of recovery is likely due to continued drought conditions. More severely  
413 burned areas may require longer recovery time as well. For the Station Fire (Figure 6c-d), we  
414 observe similar seasonal signals as for the Bobcat Fire, and also see evidence of the Bobcat Fire  
415 in 2020, as the two fires overlapped in some areas. In 2021, there does not appear to be much  
416 vegetation change within the Station Fire since 2020, and it is difficult to draw conclusions  
417 regarding recovery since there is only one data acquisition in 2009 before the fire.

### 3.5 Polarimetric Relationship to Vegetation Type

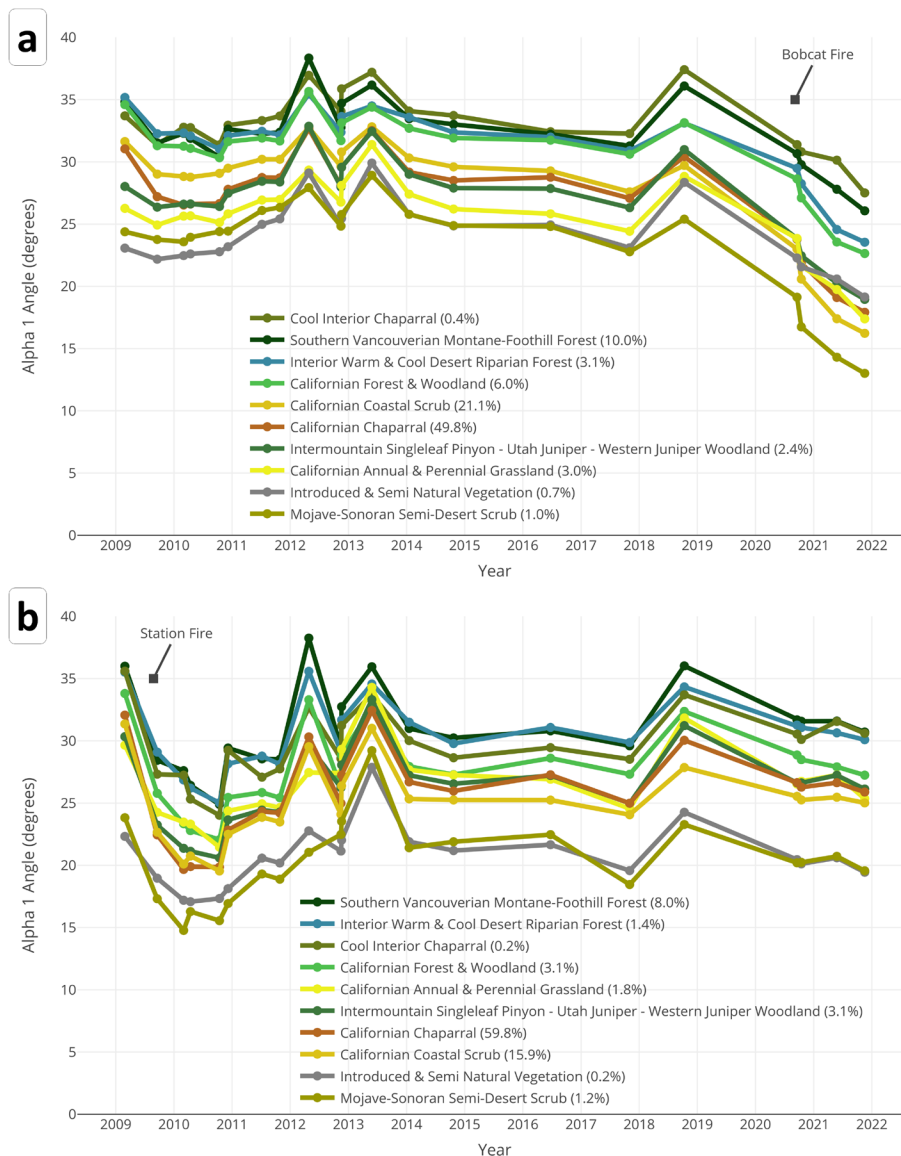


**Figure 7.** Time series of average Alpha 1 Angle for the most dominant vegetation species within the Bobcat Fire perimeter (a) and Station Fire perimeter (b). The legend lists the vegetation species name generally ordered from highest to lowest Alpha 1 Angle, and percentage area coverage is given in each legend entry.

A similar analysis to the previous alpha angle time series (Figure 7) is repeated using vegetation type instead of burn severity class. Within the Bobcat Fire, the Cool Interior Chaparral species contains the highest average Alpha 1 Angle over the full time period, but this species only covers 0.4% of the observed area (Figure 7a). The most commonly occurring species, Californian Chaparral and Californian Coastal Scrub, are observed near the middle of all species plotted, around the 30 degrees line (Figure 7a). In general, the forest species all have higher alpha angle values, indicating more volume scattering. Shorter vegetation species such as grassland and scrubs measure lower alpha angles, indicating more surface scattering, as

447 expected. The Station Fire plot displays a similar distribution of vegetation species (Figure 7b).  
448 Here, two forest species observe the most volume scattering, while Californian Chaparral and  
449 Californian Coastal Scrub have lower alpha angle values than within the Bobcat Fire. The initial  
450 starting point of these two most common species is similar for both fires, but has a lower alpha  
451 angle on average for the Station Fire because the time series observes the post-fire conditions,  
452 rather than pre-fire for the Bobcat Fire when more volume scattering should be present.  
453 Introduced semi-natural vegetation and a desert scrub show the lowest alpha angle in general for  
454 both fires. Directly following both fires, all species declined in alpha angle but at different rates.

455         The recent 2021 data acquisitions also indicate that these vegetation types have not  
456 recovered to pre-fire conditions, possibly due to continued fire and drought conditions. Overall,  
457 both fires follow the same general temporal pattern observed in Figure 6, but a separation of  
458 individual species allows for more detailed vegetation monitoring before and after a fire. Burn  
459 severity distribution also differed for each vegetation type, with shrub and forest vegetation  
460 containing the most percentage of high severity burned area (see Supporting Information, Figure  
461 S8). Thirteen percent of shrub vegetation and twelve percent of forest vegetation burned at high  
462 severity. Shrub and herb vegetation also contained higher coverage for moderately burned  
463 vegetation (62% area burned at moderate severity) compared to that of forest vegetation (36%  
464 area burned at moderate severity). The different distributions of burn severity amongst  
465 vegetation species will dictate the timing and likelihood of future regrowth patterns.

466  
467  
468  
469  
470  
471  
472  
473  
474  
475  
476  
477  
478  
479  
480  
481  
482  
483  
484

## 3.6 UAVSAR Comparison to NISAR-Simulated Data

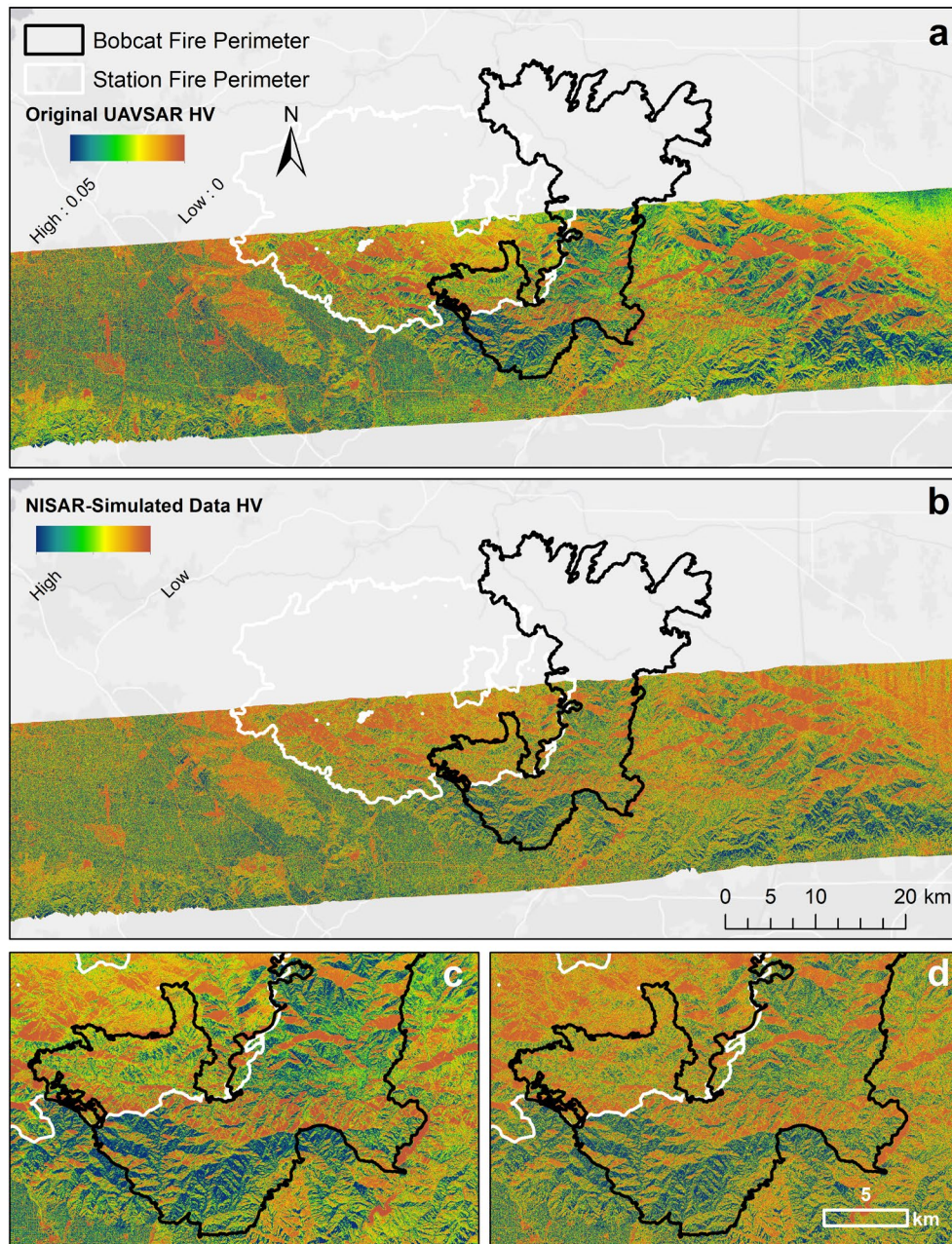


**Figure 8.** Comparison of original UAVSAR HV ground projected file (a & c) with NISAR-simulated data with 20 MHz bandwidth (b & d). Radiometric terrain correction is not performed for this comparison.

A comparison of the original UAVSAR HV ground projected product and its NISAR-simulated counterpart shows comparable quantitative results (Figures 8a-8b). RTC is not applied to either product to compare the expected image quality of NISAR as closely as possible. The products are plotted on the same colorscale and show similar broad patterns across the swath, with high returns in urban areas and certain mountainous regions. The NISAR-simulated data does show more noise (Figure 8b), as expected, and the UAVSAR data contains more detail and

contrast (Figure 8a), especially in the mountains. Within the Bobcat Fire perimeter this distinction is clearer (Figure 8c-d), with a larger range of values represented in the UAVSAR data (Figure 8c). The similarity provides promise for the ability of future NISAR products to characterize fire regimes as performed in this study.

## 4 Discussion

The original UAVSAR polarimetric products contain a wealth of information through different polarization channels and decomposition of the products. Comparison of these products with auxiliary GIS datasets help to characterize the fire regime before, during, and after a wildfire. Polarimetric radar remote sensing shows the capability of detecting current and past fire occurrence, burn severity, and tracking burn progression over time.

### 4.1 Pre-Fire Stage

Before a fire, high HV values may indicate a higher availability of fuels to burn later, and can also detect previously burned areas (showing low HV) as seen surrounding the Bobcat perimeter. The overlap areas between fires also indicate that past fire perimeters alone do not dictate the absence of future fires; the availability of current fuels is also necessary due to vegetation type and regrowth. HV images are also useful for delineating (and validating) the fire scar of these past fires as many surrounding examples follow closely, but not exactly their perimeter outlines (Figure 2). This is due to the traditionally manual (hand-drawn) generation of fire perimeters by fire agencies, which can be subject to individual interpretation and delays in reporting.



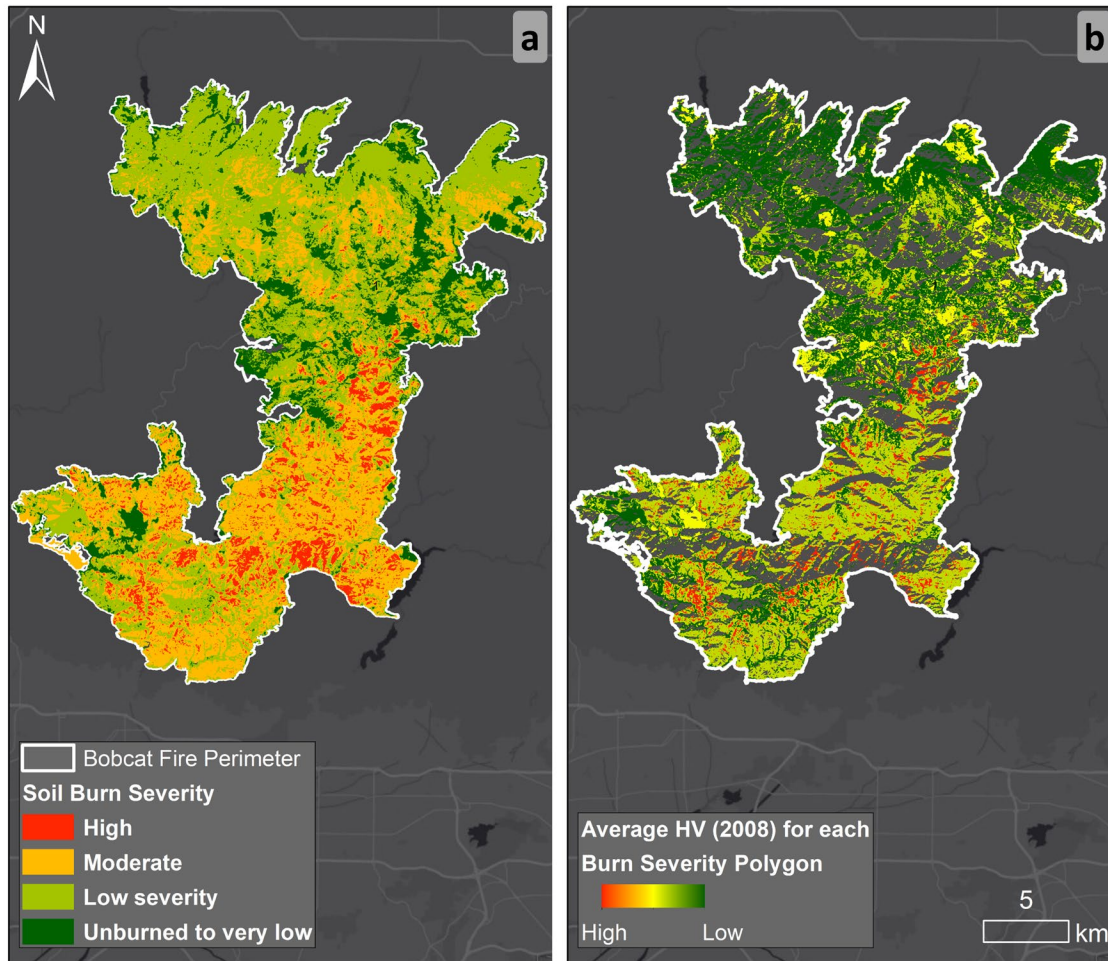


**Figure 9.** Bobcat Fire GIS soil burn severity from USDA/BAER (a) compared to the average pre-fire HV value (2018) within each burn severity polygon (b). Higher HV values pre-fire (more vegetation) correspond well to areas that experienced moderate and high burn severity. Missing areas in panel B are due to omission of data in the radar terrain shadow.

Further comparison of the HV return in 2018 and eventual soil burn severity is performed (Figure 9) using GIS tools. The burn severity raster, based on optical imagery, is converted to polygons in Esri's ArcMap (Figure 9a). For each polygon, zonal statistics calculate the average HV within each feature (Figure 9b). The high burn severity features contain the highest average HV value pre-fire in 2018. This further confirms the visual comparison (Figure 2) of high availability of fuels, not just within the Bobcat perimeter, but specifically within those areas that experienced high burn severity. The moderate burn severity areas show a lower average HV albeit higher than the values in the low burn severity areas. This relationship holds for most of the Bobcat Fire burn area. Therefore, this suggests that a knowledge of the current HV values in forested areas can offer useful fuels information for fire management, and that a threshold HV value can help to quantify fuel availability for future events. The soil burn severity map from the same data source for Station Fire can be found in the supporting information (Figure S9).

## 4.2 Active Fire Stage

A simple HV difference can offer a quick glimpse into the soil burn severity of an active fire. Burned areas show low HV return due to loss of vegetation while the surrounding areas outside the burn area show little change during the time period. Any vegetation changes, such as agricultural activities or previous fires, will also be captured in the same time period. With continuous acquisitions, subsequent HV difference images offer progress updates of the burn, only showing recently burned areas. Updating fire perimeters with the most recent information and improving upon manually generated maps can improve resource direction for fire agencies and update evacuation maps.

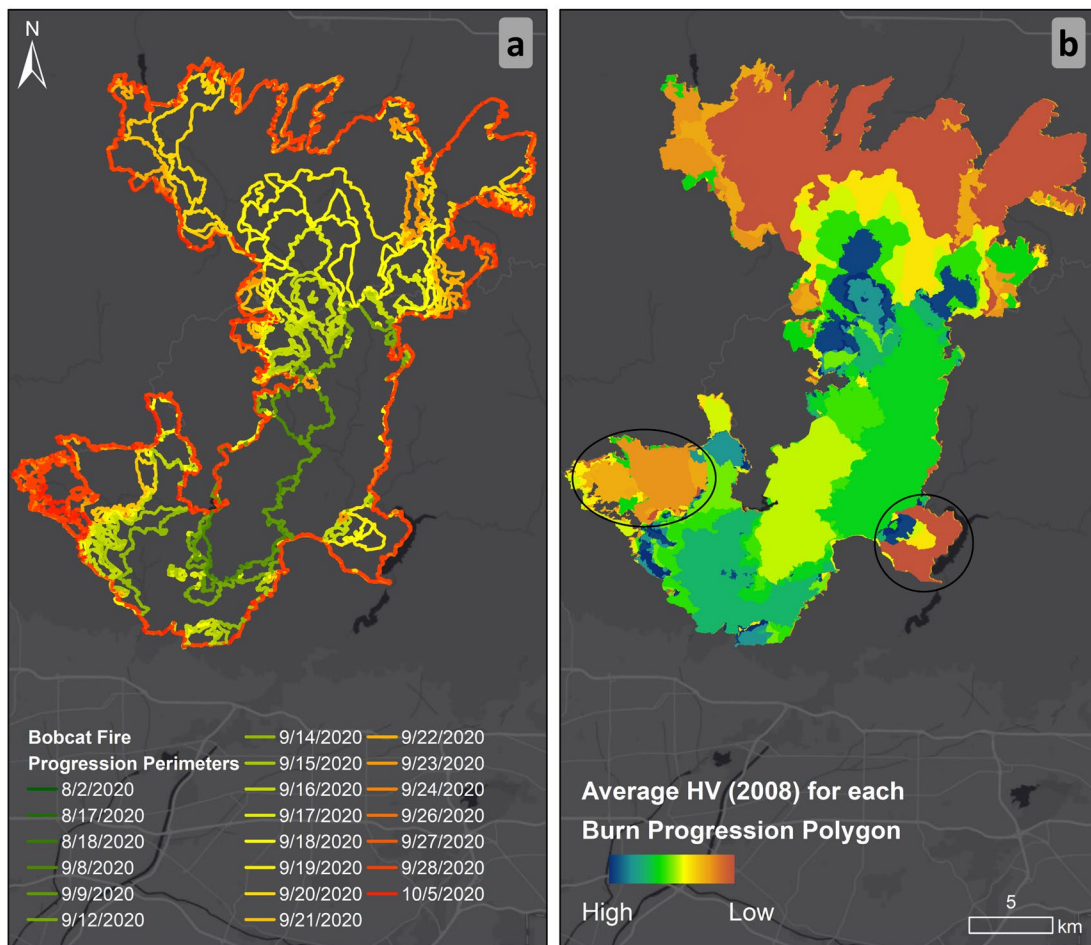


**Figure 10.** GIS fire progression perimeters for dates from August to October 2020 (a) compared to the average HV value (2018, pre-fire) within each perimeter (b). The fire perimeters (a) show where the fire started (green) and how it spread (green to yellow to red). Blue and green polygons in panel b indicate higher average HV values measured in 2018. Areas of interest discussed in the text are encircled (black).

Similar to Figure 9's burn severity comparison, burn progression can also be compared with pre-fire fuel availability (Figure 10). Green outlines (Figure 10a) indicate areas that first started burning in August 2020 and red areas burned last in October, with the Bobcat Fire officially contained in December 2020. For each progression polygon, zonal statistics is

performed to calculate the average 2018 HV value within each feature (Figure 10b). Dark blue and green polygon results (Figure 10b) identify areas which contained higher vegetation before the Bobcat Fire. In general, the center areas which burned first had higher fuel available to burn, and the fire progressed towards relatively lower fuel available areas in the north, east and west. The encircled areas towards the east and western edges are especially highlighted as burning later in time (seen in Figure 4), and these areas also have a lower average HV value before the Bobcat Fire. These areas first burned around 09/19-09/21 (Figure 10a), which aligns with the time period of the second HV difference image, 09/18-10/15 (Figure 4). A similar pattern is observed with slope, where areas that burned first tend to contain higher average slope values (see Supporting Information, Figure S7). It is likely that including a combination of vegetation fuel (HV as proxy) and slope in models could be used to identify the more likely directions of fire progression. More study is needed to understand other contributing factors, which include soil moisture and local winds, which themselves are influenced by the fire.

#### 4.3 Post-Fire Stage

A final, SAR-derived burn scar map is produced several months after the fire has been contained (Figure 5a). This final HV difference map improves upon the published fire perimeter provided by fire agencies to help inform future fire break lines and vegetation monitoring. Continuing acquisitions a year after the fire's conclusion can provide an idea of vegetation recovery or lack thereof. This information is especially pertinent for prescribed burn campaigns, which need to evaluate how vegetation type influences recovery.

#### 4.4 Fire Impact and Recovery: Relationship to Burn Severity and Vegetation Type

The polarimetric decomposition product offers a more quantified and characterized view of the fire regime that was seen in the HV images (Figure 6-7). Six polarimetric parameters (HV, Eigenvector 1, Eigenvalue 1, Entropy, Anisotropy, and Mean Alpha Angle) were compared (see Supporting Information, Figure S10) to examine differences amongst the burn severity classes. The mean HV and Eigenvector 1/Alpha Angle 1 datasets are found most useful in discerning these changes, especially in the severely burned classes. In general, the mean HV value across the burn severity classes is larger for high burn severity, indicating a higher availability of fuels to burn later. The subsequent burn severity classes follow a similar pattern, but at lower magnitudes, more or less relative to their severity levels. The high severity burn class also showed the largest decrease in HV once the fire began, followed by the other burn classes (Figure 6a). This may be due to different vegetation species in the severity classes, as well as the distribution of data within each class (e.g. high severity pixels covering a smaller area).

The most dominant scattering mechanism, quantified by Alpha Angle 1 (or Eigenvector 1), shows a similar pattern. In general, the alpha angle shows the largest decreases in the moderate and high burn severity classes, suggesting the main scattering mechanism is moving towards more surface scattering ( $0^\circ$ ) as the fire progresses and loses vegetation. The most fuels available (more volume scattering) are generally observed in the high severity class. The high and moderate intensity classes also declined in alpha angle more than the low severity and unburned classes, suggesting more severe burning can result in increased surface scattering due to loss of vegetation.

The seasonal trend in the early years of the series also shows a lag behind local climatology. The seasonal lag of alpha angle may be caused by the time needed for vegetation growth to respond to an increase or decrease in precipitation. Not only does the average

scattering mechanism in the area shift to that of more surface scattering, but the high and moderate severity classes also see the largest of these shifts. More recent acquisitions in 2021 also indicate a lack of recovery, especially in the moderate and high severity areas, which even show further decreases towards surface scattering (loss of vegetation).

Alpha Angle 1 may also be helpful in characterizing different vegetation species contributing to the corresponding eigenvectors (Figure 7). The separation of different vegetation species can help further characterize fire regimes because each species contains different ignition and combustion properties. As expected, forest species within both fires show more volume scattering over time, while grassland and desert scrub observe more surface scattering (Figure 7). The most common vegetation, chaparral and coastal scrub, fall in the middle of the scattering profiles, which can be used for species identification in changing landscapes. Although the sparse time series from UAVSAR does not allow definitive assessment of species-specific susceptibility and recovery, it does show how a regularly acquired, dense time series of PolSAR data, as expected from NISAR, can be used for this purpose.

#### 4.5 UAVSAR Comparison to NISAR-Simulated Data

Similar data to those from UAVSAR will be available from the L-band NISAR sensor, of which UAVSAR is its prototype. An early comparison of NISAR-simulated products and their UAVSAR counterparts helps researchers prepare for the known increase in noise and resolution degradation of the spaceborne product. The same features of high HV are still evident within the Bobcat Fire perimeter, although seemingly dampened due to increased noise added (Figure 8c-d). The tradeoff between decreased spatial resolution and the increased temporal resolution will be worthwhile, as NISAR will offer global coverage at regular 12-day intervals of these polarimetric radar products. The time series capability of continual acquisitions offers the opportunity for fire managers to monitor the fuels available in fire-prone areas (Figure 7a) and track vegetation regrowth and recovery after a wildfire (Figure 7b).

### 5 Conclusions

Polarimetric radar remote sensing offers fire managers supplementary information on the fire regime's fuel load, past fire scars, and vegetation recovery. Single and difference HV images can offer a spatially continuous map of vegetation scattering with much higher efficiency than field surveys and in general more complete views than optical imagery, which are impacted by clouds and smoke. An exploration of polarimetric decomposition products, including eigen parameters, further quantifies specific scattering mechanisms, which can be cross-referenced with vegetation types for detailed monitoring. The pre-fire HV intensity correlates well with burn severity for medium and high intensity classes, and can be used to focus pre-fire management. During an event, the airborne UAVSAR sensor can provide real-time measurements of burn severity and progression, seeing through the smoke and weather conditions which typically inhibit traditional surveys. Post-fire, both HV, as a proxy for vegetation, and Alpha Angle 1, as an indicator of scattering mechanisms, can track recovery by fuel type given a vegetation map.

Long-term monitoring with a similar L-band instrument can be achieved once the upcoming NISAR sensor is fully operational. This study presents the utility of only a few data acquisitions to preview consistent 12-day data products. Continuous acquisitions across the globe will allow for time series tracking of available fuel loads pre-wildfire, and vegetation recovery post-wildfire. More reliance on remote sensing methods and emerging interest in SAR-based

monitoring of wildfire is evident from recent community meetings (e.g. NASA Science Mission Directorate (SMD) Wildfire Stakeholder Engagement Workshop, 2022). Together, the airborne and spaceborne sensors potentially offer an all-encompassing fire detection and prevention tool to supplement fire agencies' current toolkit.

## Acknowledgments

The authors would like to thank Marco Lavallo (NASA Jet Propulsion Laboratory) for help correcting the PolSARpro coherency matrix generation (see Supporting Information, Text S1). Planet imagery is shown courtesy of ©Planet Labs PBC, CC BY-NC-SA 2.0. The authors acknowledge the NASA UAVSAR team for acquiring and processing the polarimetric radar data products and NISAR-simulated datasets. The UAVSAR data are courtesy of NASA/JPL-Caltech ([www.uavsar.jpl.nasa.gov](http://www.uavsar.jpl.nasa.gov)) and can be accessed through the Alaska Satellite Facility website (<https://vertex.daac.asf.alaska.edu/>). This material is based upon work supported by the Jet Propulsion Laboratory Postdoctoral Program. This research was carried out at the Jet Propulsion Laboratory, California Institute of Technology, under a contract with the National Aeronautics and Space Administration.

## Open Research

The UAVSAR HV images and NISAR-simulated data used in this study from flight lines SanAnd\_08525 and SanAnd\_08527 are available to download from the UAVSAR website (<https://uavsar.jpl.nasa.gov/cgi-bin/data.pl>). The datasets used in this study, including the HV difference maps are made available via the NASA Open Data Portal (*will link here at time of publication*). The software used to generate the Alpha Angle 1 products is PolSARpro, a toolbox available from the European Space Agency (<https://step.esa.int/main/toolboxes/polsarpro-v6-0-biomass-edition-toolbox/>). The fire perimeters can be accessed from the National Interagency Fire Center (<https://data-nifc.opendata.arcgis.com/datasets/nifc::wfigs-current-wildland-fire-perimeters/about>). Vegetation species maps are downloaded from the GAP/LANDFIRE National Terrestrial Ecosystems 2011 dataset (<https://doi.org/10.5194/isprsarchives-XL-1-245-2014>). Soil burn severity maps are downloaded from the Burned Area Emergency Response teams (<https://burnseverity.cr.usgs.gov/products/baer>).

## References

- Ban, Y., Zhang, P., Nascetti, A., Bevington, A. R., & Wulder, M. A. (2020). Near real-time wildfire progression monitoring with Sentinel-1 SAR time series and deep learning. *Scientific reports*, 10(1), 1322.
- Bekaert, D. P., Jones, C. E., An, K., & Huang, M. H. (2019). Exploiting UAVSAR for a comprehensive analysis of subsidence in the Sacramento Delta. *Remote sensing of environment*, 220, 124-134.



- Cloude, S. R., & Pottier, E. (1997). An entropy based classification scheme for land applications of polarimetric SAR. *IEEE transactions on geoscience and remote sensing*, 35(1), 68-78.
- Crockett, Joseph L., and A. Leroy Westerling. "Greater temperature and precipitation extremes intensify Western US droughts, wildfire severity, and Sierra Nevada tree mortality." *Journal of Climate* 31.1 (2018): 341-354.
- Czuchlewski, K. R., & Weissel, J. K. (2005, July). Synthetic Aperture Radar (SAR)-based mapping of wildfire burn severity and recovery. In *Proceedings. 2005 IEEE International Geoscience and Remote Sensing Symposium, 2005. IGARSS'05. (Vol. 1, pp. 4-pp)*. IEEE.
- Denbina, Michael. Radiometric terrain correction code. NASA JPL.
- Dennison, P. E., Roberts, D. A., & Reggelbrugge, J. C. (2000, February). Characterizing chaparral fuels using combined hyperspectral and synthetic aperture radar data. In *Proc. 9th AVIRIS Earth Science Workshop (Vol. 6, pp. 23-25)*. Jet Propulsion Lab.
- Fore, A., Chapman, B., Hensley, S., Michel, T., & Muellerschoen, R. (2009). UAVSAR Polarimetric Calibration.
- French, N. H., Kasischke, E. S., Hall, R. J., Murphy, K. A., Verbyla, D. L., Hoy, E. E., & Allen, J. L. (2008). Using Landsat data to assess fire and burn severity in the North American boreal forest region: an overview and summary of results. *International Journal of Wildland Fire*, 17(4), 443-462.
- Hallema, Dennis W., François-Nicolas Robinne, and Kevin D. Bladon. "Reframing the challenge of global wildfire threats to water supplies." *Earth's Future* 6.6 (2018): 772-776.
- Hensley, S., Jones, C., & Lou, Y. (2012, July). Prospects for operational use of airborne polarimetric SAR for disaster response and management. In *2012 IEEE International Geoscience and Remote Sensing Symposium (pp. 103-106)*. IEEE.
- Hensley, S., Oveisgharan, S., Saatchi, S., Simard, M., Ahmed, R., & Haddad, Z. (2013). An error model for biomass estimates derived from polarimetric radar backscatter. *IEEE Transactions on Geoscience and Remote Sensing*, 52(7), 4065-4082.
- Hislop, S., Jones, S., Soto-Berelov, M., Skidmore, A., Haywood, A., & Nguyen, T. H. (2018). Using landsat spectral indices in time-series to assess wildfire disturbance and recovery. *Remote sensing*, 10(3), 460.
- Los Angeles Times. (2019, August 26). 10 years on, the station fire remains burned into the minds of locals and fire officials. *Los Angeles Times*. Retrieved January 13, 2023, from <https://www.latimes.com/california/story/2019-08-26/station-fire-10-years-later>
- Lewis, S. A., Hudak, A. T., Ottmar, R. D., Robichaud, P. R., Lentile, L. B., Hood, S. M., ... & Morgan, P. (2011). Using hyperspectral imagery to estimate forest floor consumption from wildfire in boreal forests of Alaska, USA. *International Journal of Wildland Fire*, 20(2), 255-271.
- McKerrow, Alexa J., et al. "Integrating recent land cover mapping efforts to update the national gap analysis program's species habitat map." *The International Archives of Photogrammetry, Remote Sensing and Spatial Information Sciences* 40.1 (2014): 245.
- Moritz, M. A., Batllori, E., Bradstock, R. A., Gill, A. M., Handmer, J., Hessburg, P. F., ... & Syphard, A. D. (2014). Learning to coexist with wildfire. *Nature*, 515(7525), 58-66.

- Musgrove, Cameron H., and James C. West. "Mitigating effects of missing data for SAR coherent images." *IEEE Transactions on Aerospace and Electronic Systems* 53.2 (2017): 716-721.
- NASA Science Mission Directorate (SMD) Wildfire Stakeholder Engagement Workshop: Summary and Key Findings (February 2022).
- Nunziata, F., Ferrentino, E., Buono, A., Sarti, M., & Migliaccio, M. (2021, July). A Dual-Polarimetric Approach to Observe Wildfires Using C-Band PolSAR Measurements. In 2021 IEEE International Geoscience and Remote Sensing Symposium IGARSS (pp. 5953-5956). IEEE.
- Parker, J., Donnellan, A., & Glasscoe, M. (2021). Survey of transverse range fire scars in 10 years of UAVSAR polarimetry. *Earth and Space Science*, 8(5), e2021EA001644.
- Planet. RapidEye Imagery Products. <https://developers.planet.com/docs/data/rapideye/>
- Perry, D. A., Hessburg, P. F., Skinner, C. N., Spies, T. A., Stephens, S. L., Taylor, A. H., ... & Riegel, G. (2011). The ecology of mixed severity fire regimes in Washington, Oregon, and Northern California. *Forest Ecology and Management*, 262(5), 703-717.
- Pottier, E., & Ferro-Famil, L. (2012, July). PolSARPro V5. 0: An ESA educational toolbox used for self-education in the field of POLSAR and POL-INSAR data analysis. In 2012 IEEE International Geoscience and Remote Sensing Symposium (pp. 7377-7380). IEEE.
- Pyne, S. J. (1984). Introduction to wildland fire. Fire management in the United States. John Wiley & Sons.
- Rao, K., Williams, A. P., Flefil, J. F., & Konings, A. G. (2020). SAR-enhanced mapping of live fuel moisture content. *Remote Sensing of Environment*, 245, 111797.
- USDA Forest Service, Geospatial Technology and Applications Center, BAER Imagery Support Program (2020, November 13). Soil Burn Severity Dataset for the BOBCAT Fire occurring on the Angeles National Forest National Forest. Salt Lake City, Utah, USA: USDA Forest Service. Accessed at: <https://fsapps.nwcg.gov/afm/baer/download.php> [Dataset]
- Simard, Marc, et al. "Radiometric correction of airborne radar images over forested terrain with topography." *IEEE Transactions on Geoscience and Remote Sensing* 54.8 (2016): 4488-4500.
- U.S. Forest Service (Angeles National Forest). Bobcat Fire Incident Overview. Accessed at: <https://inciweb.nwcg.gov/incident/7152/>
- U.S. Geological Survey (USGS) Gap Analysis Project (GAP) (2016). GAP/LANDFIRE National Terrestrial Ecosystems 2011: U.S. Geological Survey. Accessed at: <https://doi.org/10.5066/F7ZS2TM0>. [Dataset]
- Van Wagendonk, J. W., Root, R. R., & Key, C. H. (2004). Comparison of AVIRIS and Landsat ETM+ detection capabilities for burn severity. *Remote sensing of environment*, 92(3), 397-408.
- Veraverbeke, S., Verstraeten, W. W., Lhermitte, S., & Goossens, R. (2010). Evaluating Landsat Thematic Mapper spectral indices for estimating burn severity of the 2007 Peloponnese wildfires in Greece. *International journal of wildland fire*, 19(5), 558-569.
- Westerling, A. L., Hidalgo, H. G., Cayan, D. R., & Swetnam, T. W. (2006). Warming and earlier spring increase western US forest wildfire activity. *science*, 313(5789), 940-943.

756 Wildland Fire Interagency Geospatial Services (WFIGS) Group, National Interagency Fire  
757 Center (2022). Wildland Fire Perimeters Full History. Accessed at: [https://data-](https://data-nifc.opendata.arcgis.com/datasets/nifc::wfigs-wildland-fire-perimeters-full-history/about)  
758 [nifc.opendata.arcgis.com/datasets/nifc::wfigs-wildland-fire-perimeters-full-history/about](https://data-nifc.opendata.arcgis.com/datasets/nifc::wfigs-wildland-fire-perimeters-full-history/about).  
759 [Dataset]  
760